Journal of The Electrochemical Society, **161** (4) C215-C222 (2014)
0013-4651/2014/161(4)/C215/8/$31.00 © The Electrochemical Society

Synergistic Protection against Corrosion of AA2024-T3 by Sol-Gel Coating Modified with La and Mo-Enriched Zeolites

S. A. S. Dias,[a,b,z] S. V. Lamaka,[b] T. C. Diamantino,[a] and M. G. S. Ferreira[b,c,*]

[a]*Laboratório Nacional de Energia e Geologia (LNEG), 1649-038 Lisboa, Portugal*
[b]*ICEMS, Instituto Superior Técnico, Universidade de Lisboa, 1049-001 Lisboa, Portugal*
[c]*CICECO, DEMaC, Universidade de Aveiro (UA), 3810-193 Aveiro, Portugal*

The present work demonstrates an improvement in corrosion protection of sol-gel coatings modified with a mixture of lanthanum and molybdate-enriched zeolite microparticles (La+Mo) due to synergistic effect between lanthanum and molybdate. The effect of these inhibitor species on protection of AA2024-T3 substrate has been studied by Electrochemical Impedance Spectroscopy and Localized Electrochemical Impedance Spectroscopy. Both techniques revealed an enhanced protection when compared with the case where the inhibitors were used alone. The inhibiting mechanism could involve on demand release of molybdate and lanthanum ions from the loaded zeolite followed by the formation of molybdenum oxide/hydroxide and a Mo-Na-La compound on intermetallic particles.

Manuscript submitted November 19, 2013; revised manuscript received February 4, 2014. Published February 19, 2014.

One of the most common strategies used by corrosion engineers to protect metallic structures against corrosion degradation is the application of protective coatings. Organic coating systems have been widely used and consist of several "coating" layers where each one has a specific action. Hybrid sol-gel films have been extensively studied during the last decade as a possible pre-treatment/primer layer[1,2] for different materials and alloys and used as model matrix for different encapsulated corrosion inhibitors.[3–10] However, these films have low thickness and do not provide a suitable barrier effect. Formation of cracks or other type of defects initiate a more pronounced disruption of the barrier properties leading to corrosion.[2,3] In order to provide the desirable protection performance of sol-gel coatings, the addition of corrosion inhibitors (such as cerium or lanthanum)[11,12] is necessary.[13] However, the simplest way of introduction of the inhibiting species, direct addition to the sol-gel formulation, proved to be unsuitable for high concentration of the species due to interaction with the film matrix leading to an early destruction of the barrier effect.[14] For example, the protection of sol-gel film doped with $Ce(NO_3)_3$ is only observed if the amount of Ce^{3+} is in the 0.2 to 0.6 wt% range.[14] Alternative approaches with encapsulation of inhibitors in nano-/micro-containers[3–10,15–17] have been tried to enhance the protection properties of the sol-gel coatings without disrupting the barrier effect of the film. Among these, one successful approach has been the use of zeolite microparticles loaded with inhibitor species.[7,9,10] Considerable improvement of protective performance has been achieved in sol-gel coatings modified with a mixture of cerium and molybdate-enriched zeolite microparticles (Ce+Mo coating)[10] and a sol-gel modified with cerium-enriched zeolite (Ce-NaX coating).[7,9] Experimental evidence showed that there is a controlled release of cerium and molybdate ions, in response to the adsorption of Mg^{2+}[10] and Cu^{2+}[9] by ion-exchange reactions, followed by their precipitation on intermetallic (IM) particles[9,10] slowing down the corrosion activity. In fact, the significant improvement observed on protection performance with Ce+Mo coating was due to a synergistic effect between the two species released on demand from the loaded zeolites. Otherwise it would not be possible to accomplish the formation of a stable molybdenum containing-oxide/hydroxide film on the IM particles and the behavior of this coating would be similar to the sol-gel film modified only with Mo-enriched zeolite only or Ce-enriched zeolite.[10] Experimental evidence also showed that zeolite-enriched microparticles have the ability to adsorb Cl^- ions from the electrolyte solution.[9]

The aim of this work is to exploit possible synergistic effect between lanthanum and molybdate and their respective inhibiting mechanisms in sol-gel modified with a mixture of lanthanum and molybdenum-enriched zeolite microparticles. The enriched-zeolite microparticles were characterized by energy-dispersive X-ray fluorescence technique (EDXRF) and X-ray diffraction (XRD). Scanning electron microscopy coupled with energy dispersive X-ray spectroscopy (SEM/EDS) was also used to characterize the zeolite microparticles, the surface and cross-section of the developed sol-gel coatings modified with the zeolite microparticles before and after the electrochemical tests. The protection performance was assessed by electrochemical impedance spectroscopy (EIS) and localized electrochemical impedance spectroscopy (LEIS) measurements. The release of La and Mo-containing species from inhibitor enriched-zeolite microparticles was studied by EDXRF and atomic absorption spectrometry (AAS).

Experimental

Materials.— AA2024-T3 aluminum alloy plates were used in this study as metallic substrate. All panels were chemically etched before application of the coatings. An industrial-like three-step cleaning procedure consisting of alkaline cleaning in Metaclean T2001 at 60 ± 10°C for 18 min, followed by alkaline etching in P3 Almeco at 30 ± 10°C for 3 min and then acid etching in Turco Liquid Smutgo NC at 30 ± 5°C for 3 min. Finally the panels were rinsed with distilled water.[7]

Zeolite microparticles (NaX) were obtained from Sigma-Aldrich (Ref. 283592, $Na_xAl_{58}Si_{134}O_{384}.zH_2O$, 13X). The Si/Al molar ratio of the particles was 1.23 and the average particle size < 2 μm. Lanthanum-enriched zeolite microparticles (LaNaX) were prepared by ion-exchange reaction of NaX with 0.1 M solution of lanthanum (III) nitrate hexahydrate (Sigma-Aldrich, 99.999%). The reaction took place in $NaNO_3$ solution (NaOH of Riedel deHaën, analytical reagent and HNO_3 of Riedel deHaën, min. 65%) with a volume/solid ratio (V/P) = 20 (in mL/g) at 80°C for 3 h. Then, the microparticles were filtered, washed with de-ionized water (in a volume five times higher than the volume of the solution used for ion-exchange) and dried during 10 hours at 100°C in an oven (Heraeus, model UT-5042). The La concentration in the LaNaX zeolite microparticles was determined by EDXRF. The crystalline structure of the ion-exchanged powders was controlled by XRD.

Molybdate-enriched zeolite microparticles (MoNaX) were prepared by incipient impregnation of NaX zeolite microparticles with 0.1 M solution of ammonium heptamolybdenum ($(NH_4)_6Mo_7O_{24} \cdot 4H_2O$) as reported in.[10] The reaction took place in $NaNO_3$ solution with a volume/solid ratio (V/P) = 1.5 (in mL/g) at room temperature during 24 h. Then, the microparticles were filtered, washed with de-ionized water (in a volume five times the volume of the solution used for ion-exchange) and dried during 10 hours.

*Electrochemical Society Active Member.
[z]E-mail: susana.dias@lneg.pt

To study the response of inhibitor-enriched zeolite particles in a coating, the ZrO_2/SiO_2 sol-gel coating was selected.[3,4] The addition of 2 wt% commercial (NaX) or modified zeolite microparticles to the sol-gel was performed after the aging step of the hybrid sol-gel solution. To ascertain the contribution of each component regarding the protective properties of the film modified with zeolites, five types of formulations were prepared:

- blank – AA2024-T3 substrate coated with sol-gel film only;
- NaX – AA2024-T3 substrate coated with sol-gel film modified with commercial zeolite microparticles (2 wt%);
- LaNaX– AA2024-T3 substrate coated with sol-gel film modified with LaNaX zeolite microparticles (2 wt%);
- MoNaX– AA2024-T3 substrate coated with sol-gel film modified with MoNaX zeolite microparticles (2 wt%);
- La+Mo – AA2024-T3 substrate coated with sol-gel film modified with a mixture of 1 wt% of LaNaX and 1 wt% of MoNaX zeolite microparticles.

With the purpose of eliminating variations introduced by different production batches and to ensure the repeatability of performance of the modified sol-gel coatings, all samples were prepared and coated simultaneously.

Characterization.—Morphological and chemical characterization.— The amount of La loaded in zeolite microparticles (LaNaX) was determined by measuring La concentration in the preparation solution before and after the exchange reaction. An EDXRF spectrometer Spectrace QuanX was used with the following acquisition parameters: 11 kV, 0.16 mA, cellulose filter; time 70 s. The region of interest (ROI) considered for peak intensity determination of La was in the range 4.34 to 4.86 keV corresponding to the Lα transition.

The determination of molybdenum concentration in zeolite microparticles was performed by AAS (GBC 906AA, Australia) using the following procedure. Samples of about 0.5–1 g of zeolite were rigorously weighed and digested with nitric acid (analytical grade from Panreac) on a hot plate for 30 minutes. The resultant solutions were filtered and washed into volumetric flasks and the volume adjusted. If necessary, dilutions were performed according to the calibration range used (standards from 2 to 15 mg/L Mo, prepared from 1 g/L Merck standard solution). The solutions were then analyzed by AAS with a N_2O/acetylene flame, at 313.3 nm wavelength and 0.2 nm slit width.

To measure the amount of La and Mo ions released from the zeolites at different pHs, samples were prepared with a V/P = 20 of La and molybdate-enriched zeolites microparticles and were immersed in 0.5 M NaCl solution. The pH of solution was preliminary adjusted with nitric acid (pH range between 2 and 4) and with sodium hydroxide (pH range of 6 to 8.6). After 48 hours of immersion, the zeolites microparticles were separated by filtering. The concentrations of La and Mo ions in solution were measured by EDXRF and AAS, respectively.

The microstructure and chemical composition of the zeolite microparticles and hybrid sol-gel coatings, before and after the immersion tests, were studied by SEM/EDS. A Philips XL30 FEG microscope was used. The samples for cross-section analysis were prepared by embedding the samples in epoxy resin (Acryfix, Struers) followed by polishing. All samples were coated with gold film of few angstroms of thickness by sputtering technique in order to make the surfaces conductive.

The crystalline structure of zeolite powders was characterized by XRD using a Rigaku-Geigerflex diffractometer (Model-D/MAX III C, Japan) with a Ni-filtred Cu Kα radiation (λ = 0.1506 Å) in an angular range 2θ = 5 to 50°, at 1.2°2θ min^{-1} and steps of 0.012.

*Electrochemical tests.—*The protection performance of artificial "damaged" sol-gel coatings was evaluated by EIS for 2 weeks of immersion in 0.05 M NaCl solution. Artificial defects, scratches, were produced by a Vickers micro-indenter with a diamond pyramidal tip with penetration to the metallic substrate.

The measurements were carried out using a Gamry FAS2 Femtostat coupled with a PCI4 Controller at open circuit potential, by applying a 10 mV sinusoidal perturbation in the range of 60 kHz to 1 mHz; 9 experimental points were collected per frequency decade. A conventional three-electrode cell was used consisting of a saturated calomel reference electrode (SCE), a coiled platinum wire as counter electrode and the sol-gel coated AA2024-T3 substrate as working electrode with an area of 3.14 cm^2. All measurements were performed in a Faraday cage in order to avoid electromagnetic interference. At least four samples were measured for each type of coating to check the repeatability of results. Zview software, version 3.30, was used to fit the impedance spectra.

LEIS measurements were carried out with a Solartron 1286 system. This method used a five-electrode configuration composed by the sample, a platinum mesh as the counter-electrode, a SCE (sat. KCl) reference electrode and a Uniscan probe with two electrodes. The specification and modification of the commercial probe were described elsewhere.[9] The experiments were carried out in 1×10^{-3} M NaCl (κ = 0.2 mS/m) in order to improve the resolution of the method. For local electrochemical impedance scanning an excitation frequency of 77 Hz was chosen. LEIS measurements were acquired stepwise every 15 μm across a line of 1500 to 4000 μm perpendicular to the scratch. At least two replicates were performed for each type of coating to check the repeatability of results. For clarity reasons, admittance was plotted rather than impedance.

Calculation of synergistic parameters.— The inhibition efficiency (*IE*) of an inhibitor can be determined by:

$$IE = (CR_0 - CR_{inh})/CR_0 = ((1/R_{ct})_0 - (1/R_{ct})_{inh})/(1/R_{ct})_0 \quad [1]$$

where $(R_{ct})_0$ is the charge transfer resistance in solution without inhibitor (3% NaCl) and $(R_{ct})_{inh}$ is the same parameter for the same solution containing inhibitor.

The synergistic parameter (*S*) of the mixture of the two inhibitors[18] is given by

$$S = (1 - IE_{1+2})/(1 - IE_{12}) \quad [2]$$

where IE_{12} is inhibition efficiency parameter of the coating modified with both inhibitors and $IE_{1+2} = (IE_1+IE_2)-(IE_1.IE_2)$. The inhibition efficiencies, IE_1, IE_2 and IE_{1+2} are calculated for inhibitors 1, 2 and the mixture of both, respectively.

The concept of synergistic effect behavior was, in this paper, extended to the mixture of inhibitors in a same coating and means the gain in protection due to the cooperative effect resulting from the presence of both inhibitors, when this protective effect is higher than the addition of those conferred by each inhibitor when used separately. The synergistic behavior of the mixture of the two inhibitors is observed when the value of $S > 1$.[18,19]

Results and Discussion

Characterization of the sol-gel coatings.— Figure 1 shows SEM micrographs of the sol-gel modified with the mixture of LaNaX and MoNaX zeolite microparticles (La+Mo). In the micrographs of Figure 1a and 1b it is possible to observe the distribution of zeolite microparticles in the sol-gel matrix. Although there are some areas with zeolite agglomeration (zone identified with 5 in Figure 1b) where it is possible to see in the cross section micrograph (Figure 1a), that the integrity of the sol-gel matrix is not disrupted by adding the zeolite microparticles (no defects or failures are observed). The sol-gel film is adherent to the metallic substrate with a thickness between 2.7 and 3 μm (Figure 1a) and the EDS analysis on the areas 2 only presents the structural elements of sol-gel matrix (C, O, Si and Zr elements) (Figure 1(d2)).

The EDS analysis on white zones, marked with 1 in Figure 1a, identified O, Al and Si elements from the zeolite structure, with Na and La as the loaded counter-cations of the zeolite and C and Zr elements from the sol-gel matrix (Figure 1(d1)).

Another fact worth mentioning is the existence of acicular shapes (zone identified with 3 in Figure 1b and 1c) distributed preferentially close to Cu-rich areas (areas identified with 4, 5 and 6 (Figure 1b

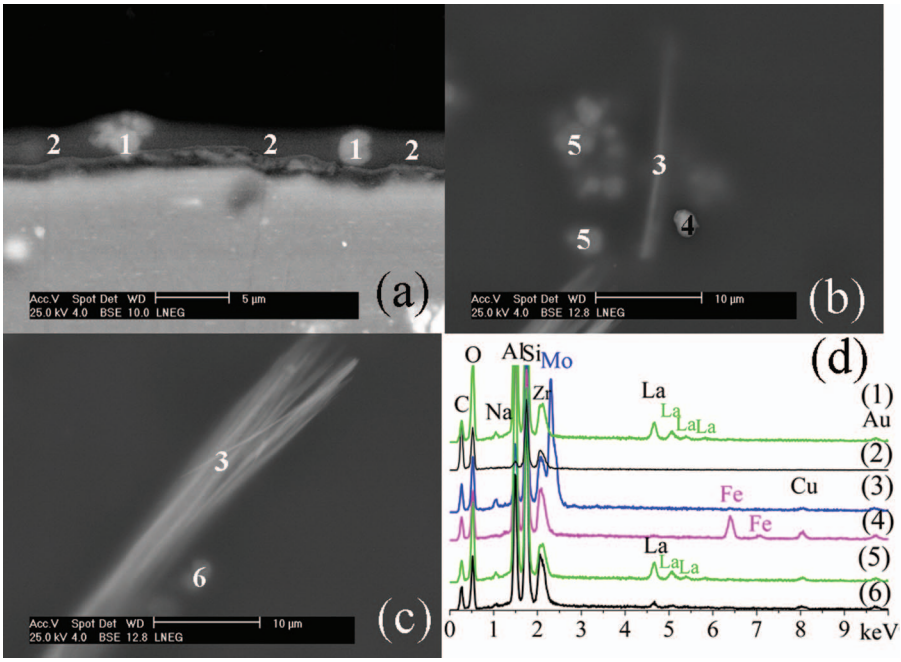

Figure 1. SEM/EDS analyzes of AA 2024 coated with hybrid sol-gel film modified with LaNaX and MoNaX zeolite microparticles (a) Cross section, (b),(c) longitudinal micrographs and (d) EDS analysis on (1),(5),(6) La-enriched zeolite microparticles, (2) sol-gel film, (3) acicular structure and (4) intermetallic particle.

and 1c). This preferential distribution was already observed in our previous work.[10] EDS analyzes identified these acicular structures as a molybdenum-sodium containing compound (Figure 1(d3)). Their presence was expected due to the presence of two crystalline phases with molybdenum in the diffraction pattern of MoNaX zeolite powder (Figure 2). The diffraction pattern of MoNaX zeolite microparticles identified three different crystalline phases, NaX,[20] ammonium molybdenum oxide ($(NH_4)_2Mo_3O_{10}$)[21] and sodium molybdenum oxide (Na_2MoO_4),[22] whereas the diffraction pattern of LaNaX zeolite only identified the presence of NaX crystalline phase. The presence of $(NH_4)_2Mo_3O_{10}$ in MoNaX powder can be explained by a solubility effect of the reagent - $(NH_4)_6Mo_7O_{24}.4H_2O$, due to the small volume of solution (V/P = 1.5) used in the loading process of the zeolite. However, the presence of a stable Na_2MoO_4 compound, normally formed between 713 and 863 K range,[22] is only possible due to the binding between the (NH_4) group of $(NH_4)_6Mo_7O_{24}.4H_2O$ and the atoms of the zeolite lattice.

Although the diffraction patterns of MoNaX and LaNaX zeolite microparticles are similar, apart from the identified Mo containing compounds, a pronounced overall decrease of relative intensities is observed of the individual reflections in the LaNaX diffraction pattern, apart from two exceptions at 12.25 and 14.088°2θ where there is an increase of the relative peak intensities (Figure 2). The appearance

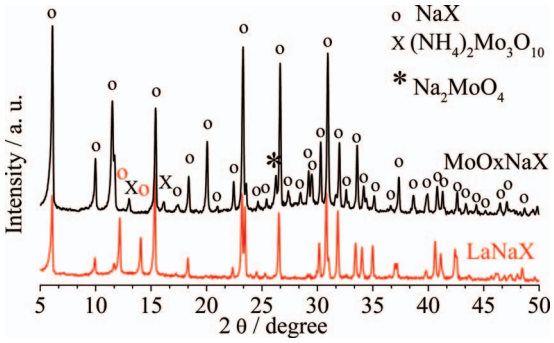

Figure 2. Diffraction patterns of Mo- and La- enriched zeolite microparticles' powders and identification of the individual reflections of NaX (open circle symbol),[20] $(NH_4)_2Mo_3O_{10}$ and Na_2MoO_4 (X,* symbols, respectively) crystalline phases.[21,22]

of the ⟨222⟩ peak at 12.25°2θ is explained by the presence of water molecules inside the zeolite structure.[23] The increase of ⟨400⟩ peak at 14.088°2θ is a consequence of an alteration in the structure factor of the crystalline matrix with the introduction of a bigger atom inside the zeolite structure.[23]

The general decrease of the relative intensity and the consequent distortion of the crystalline matrix observed in the diffraction pattern of LaNaX microparticles is a clear indication of the presence of lanthanum inside the zeolite structure and reflects the concentration of the cation in the crystalline structure.[23] The EDXRF measurements showed an overall lanthanum concentration of 18.2 wt% in LaNaX zeolites while the AAS measurements showed an overall molybdenum concentration of 1.48 wt% in MoNaX zeolite microparticles.

For the determination of inhibitor concentration in sol-gel films, the AA2024 panels were measured and weighed after the steps of surface treatment and the coating application. All coating formulations had a 26.9 wt% concentration of zeolite microparticles (dry coating). Table I shows the concentrations of La and Mo loaded on zeolite microparticles in the coatings under study.

Protective performance of sol-gel modified with zeolite microparticles.—EIS measurements.—To evaluate the performance of the active components in corrosion protection and the possibility of a cooperative effect between La^{3+} and molybdate ions released from enriched zeolites, EIS measurements were performed on zeolite loaded sol-gel coatings with an artificial scratch, of 1 mm × 65 µm down to the metallic substrate. The Bode plots of NaX, LaNaX, MoNaX and La+Mo coatings with an artificial scratch after 2 weeks of immersion in 0.05 M NaCl solution are shown in Figure 3. La+Mo

Table I. Concentration of La and Mo species loaded on zeolite microstructures in the different coating formulations.

	Inhibiting species loaded on zeolite microparticles	
Coating	La / wt%	Mo / wt%
NaX	–	–
LaNaX	~56	–
MoNaX	–	~0.4
La+Mo	~2.8	~0.2

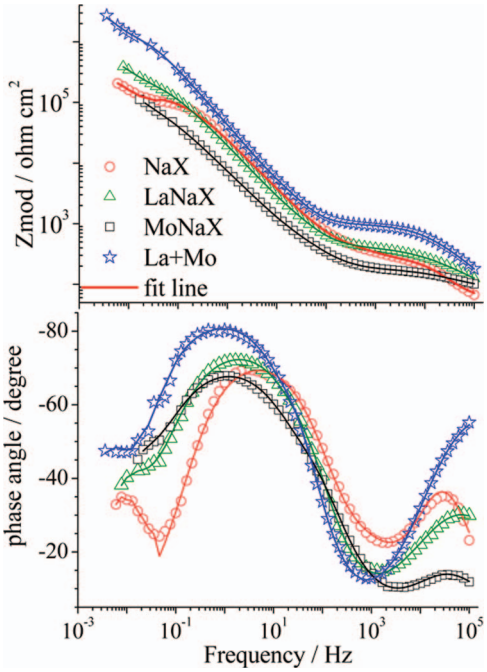

Figure 3. Bode plots of sol-gel coatings modified with NaX, LaNaX, MoNaX and LaNaX+MoNaX (La+Mo), with an artificial scratch, after 2 weeks of immersion in 0.05 M NaCl solution.

coating shows the highest values of impedance in the whole spectrum frequency range.

The corrosion protection is usually assessed from the impedance values at the lower spectrum frequency range. For a frequency of 0.01 Hz the La+Mo coating shows the highest impedance value (1.4 $\times$ 10^6 Ωcm^2) followed by the LaNaX coating with 3.4 $\times$ 10^5 Ωcm^2; NaX and MoNaX coatings show 1.6 $\times$ 10^5 Ωcm^2 and 1.5 $\times$ 10^5 Ωcm^2, respectively. The difference in impedance between the coating modified with the mixture of zeolites (La+Mo) and the remaining formulations is about one order of magnitude. The enhancement of protection efficiency of a mixture of CeNaX and MoNaX zeolites was shown previously,[10] although the difference of impedance values between Ce+Mo and CeNaX coatings is lower than the one observed in the present study for La+Mo and LaNaX coatings. One possible explanation for this fact is that Ce cations have a higher inhibiting effect on the corrosion process of AA2024 than La^{3+} species.[11,24]

For a quantitative estimation of the corrosion protection the experimental EIS data were fitted using the equivalent circuit showed in Figure 4. $R_{sol.}$ is the solution resistance; R_{pore}, R_{oxide} and R_{ct} are the pore resistance of the sol-gel coating, resistance of intermediate oxide layer and charge transfer resistance, respectively. $CPE_{coat.}$, CPE_{oxide} and CPE_{dl} are constant phase elements for sol-gel coating, intermediate oxide layer and double layer, respectively. Constant phase elements were used here instead of pure capacitances since the phase angle was not equal to $-90°$. The fitting lines are the solid lines depicted in the Bode plots (Figure 3) and the fitting parameters used are presented in Table II.

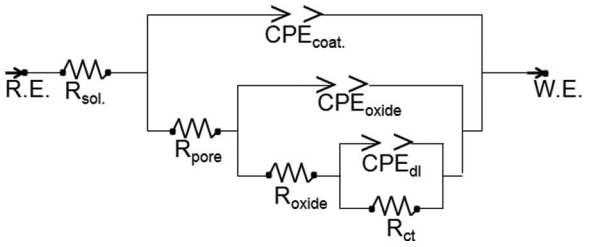

Figure 4. Equivalent circuit used to fit the experimental EIS data (R.E. reference electrode, W.E. working electrode; CPE: constant phase element; R: resistance, sol.: solution, pore: coating, oxide: intermediate oxide layer, dl: double layer and ct: charge transference).

La+Mo coating presents higher values of R parameters compared to all other coatings, followed by the LaNaX coating. The values for La+Mo coating are at least one order of magnitude higher than for the other coatings.

Optical photographs of all coating formulations are presented in Figure 5. La+Mo coating shows the artificial scratch and the whole surface without corrosion products on the surface after two weeks of immersion. Although the remaining coatings show deposition of corrosion products around the artificial scratch, the NaX coating shows the formation of several pits. However, only, the LaNaX and MoNaX coatings show a gray surface aspect. These results are in agreement with the impedance results.

Figure 6 shows the evolution of pore resistance (R_{pore}), resistance of intermediate oxide layer (R_{ox}) and charge transfer resistance (R_{ct}) of all coating formulations during 336 hours (2 weeks) of immersion in 0.05 M NaCl solution.

During the initial 7 hours of immersion all coatings showed similar R_{pore} values. The NaX coating at 4 hours immersion presented the highest value of R_{pore} and the MoNaX coating the lowest of all coatings under study. After 24 hours of measurements two trends were identified, the coatings modified with LaNaX zeolite (only or mixture) showed a stabilization of R_{pore} during the remaining time, while the other coatings showed a continuously decrease of the R_{pore} values.

Although all coatings showed an overall decrease or stabilization of the R_{pore} values, the evolution of R_{ox} and R_{ct} seems to be directly related to the action of the inhibiting species loaded on zeolite microparticles. The coatings modified with the LaNaX zeolite (La+Mo and LaNaX) showed the highest values of all coatings. In fact, it is possible to observe in La+Mo coating that there was an increase of R_{ox} values after 5 hours of immersion followed by stabilization while

Table II. Parameters and errors for the developed sol-gel coating/substrate systems obtained from fitting of the experimental impedance spectra with the equivalent circuit, showed in Figure 4; after 2 weeks of immersion in 0.05 M NaCl.

Coatings	NaX	LaNaX	MoNaX	La+Mo
R_{sol} / Ωcm^2	47.7 ± 2.8	–	83.7 ± 4.4	–
Q_{coat} / μScm^{-2}	1.0 ± 0.3	3.5 ± 0.4	2.3 ± 1.3	0.3 ± 2.6 × 10^{-2}
n_{coat}	0.76	0.56	0.71	0.73
R_{pore} / Ωcm^2	318 ± 12	442 ± 7	99 ± 8	1013 ± 10
Q_{ox} / μScm^{-2}	7.4 ± 0.3	8.4 ± 0.3	30.7 ± 1.3	4.1 ± 4.1 × 10^{-2}
n_{ox}	0.83	0.87	0.77	0.92
R_{ox} / $k\Omega cm^2$	13 ± 2	410 ± 29	213 ± 7	1812 ± 56
Q_{dl} / μScm^{-2}	16.6 ± 5.6	59.4 ± 5.9	205.1 ± 40.9	17.4 ± 0.8
n_{dl}	0.99	0.99	0.99	0.99
R_{ct} / $k\Omega cm^2$	237 ± 10	434 ± 60	300 ± 58	3856 ± 393
goodness	3.3 × 10^{-3}	2.1 × 10^{-3}	1.8 × 10^{-3}	2.2 × 10^{-3}

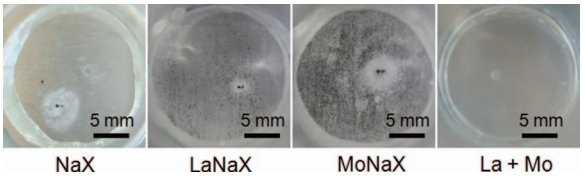

Figure 5. Optical photographs of all coatings with an artificial scratch after 2 weeks of immersion in 0.05 M NaCl solution.

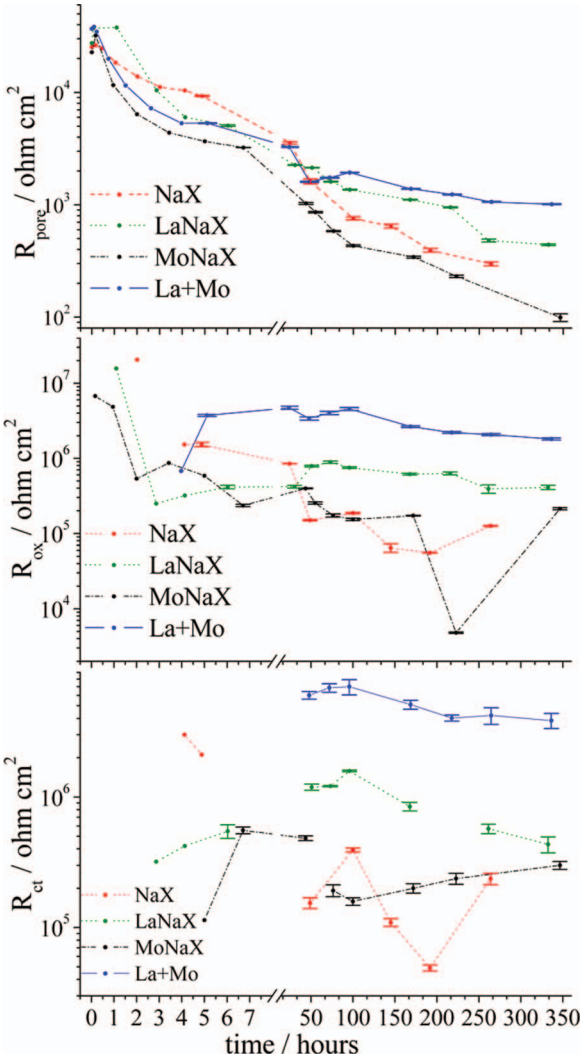

Figure 6. Evolution of the estimated pore resistance (R_{pore}), intermediate oxide layer resistance (R_{ox}) and charge transfer resistance (R_{ct}) of NaX, LaNaX, MoNaX and La+Mo coatings, with an artificial scratch, after 336 hours of immersion in 0.05 M NaCl solution (error bars correspond to the deviations of the estimated values of resistances).

for LaNaX coating an increase of R_{ox} was observed at 48 hours of immersion. The R_{ct} evolution of LaNaX coatings showed the same trend as the R_{ox}. This behavior is a clear indication that there was a slowing down of the corrosion activity and consequently there was a release of inhibiting species from the zeolite microparticles contained in the sol-gel matrix.

On the contrary, the NaX and MoNaX sol-gel coatings showed the lowest values of R_{pore} and R_{ox} during most of the EIS measurements. Several works showed that when the concentration of molybdate anion is insufficient for a total suppression of the oxygen reduction reaction, it promotes an acceleration of the corrosion activity[25–27] due to the formation of "active-passive" cells.[28] Nevertheless the sol-gel coating modified with a mixture of zeolites (La+Mo) presented the highest protection performance of all coating formulations giving a clear indication that the inhibiting mechanism in this coating is different from the expected with only La^{3+}[11,29] in LaNaX coating.

To ascertain the potential of the cooperative interaction of lanthanum and molybdate in the improvement of corrosion protection, the synergistic parameters after 1 and 2 weeks of immersion were determined (Table III). The efficiency factors (IE_n) (with eq. 1) and the synergistic parameters (S) (using eq. 2) were determined with the R_{ct} estimated from fitting of the EIS data (in 0.05 M NaCl).

The S values are higher than 1 and consequently there is a synergistic effect for both immersion times. The calculated values of S ($S = 4.18$ and 7.01 for 1 and 2 weeks of immersion, respectively) increased during the immersion allowing to conclude that the cooperative effect between La^{3+} and molybdate ions increased during the test. This effect was associated before[9,10] to the release of inhibiting species from the zeolite microparticles in the sol-gel matrix.

LEIS measurements.—LEIS measurements on all coating formulations were carried out for a better clarification of the corrosion protection mechanism of the systems under study. Figure 7 shows the evolution of the admittance modulus in a direction perpendicular to the scratch length of blank (sol-gel film only), LaNaX, MoNaX and La+Mo coatings during 1 day of immersion in 10^{-3} M NaCl solution. The dimensions of the artificial scratch were produced taking in account the probe's lateral resolution;[9] they were performed by a micro-indenter with dimensions of 2 mm × 117 μm with penetration to the metallic substrate. Depending on the coating formulation it is possible to observe in Figure 7 four types of behaviors over the scratch. Although the blank coating shows a progressive increase of the admittance values until a maximum admittance value after 6 hours of immersion (Figure 7a) the MoNaX coating (Figure 7b) shows an increase of admittance value after 2 hours of immersion followed by a decrease, recovering after 4 hours the value observed for 1 hour of immersion, but increasing again for 25 hours. A second behavior is observed for LaNaX coating (Figure 7c) where after 2 hours of immersion the admittance values progressively decrease to a minimum at 18 hours remaining stable until 24 hours of immersion. The decrease of admittance was not observed in the blank coating. This behavior reveals that there was an effective slowing down of the corrosion process due to the release of La^{3+} from the loaded zeolite microparticles followed by its precipitation on the active areas.[11,29]

A fourth behavior is observed on La+Mo coating (Figure 7d). Contrary to the other coating formulations the admittance is very low for the initial 21 hours of the test. After 22 hours of immersion the beginning of corrosion activity is observed (Figure 7d) and for longer times the progressive decrease of the admittance occurs again.

Table III. Estimated charge transfer resistance (R_{ct}), efficiency factors (IE_n) and synergistic parameters (S), after 1 and 2 weeks of immersion, in 0.05 M NaCl solution for all coatings formulations with an artificial scratch.

		Coating	R_{ct} (kΩcm^2)	IE_n	S		R_{ct} (kΩcm^2)	IE_n	S
0.05 M NaCl	1 week	Nax	109	0.00		2 weeks	237	0.00	
		LaNaX	845	0.87			434	0.45	
		MoNaX	158	0.31			300	0.21	
		La+Mo	5108	0.98	4.18		3856	0.94	7.01

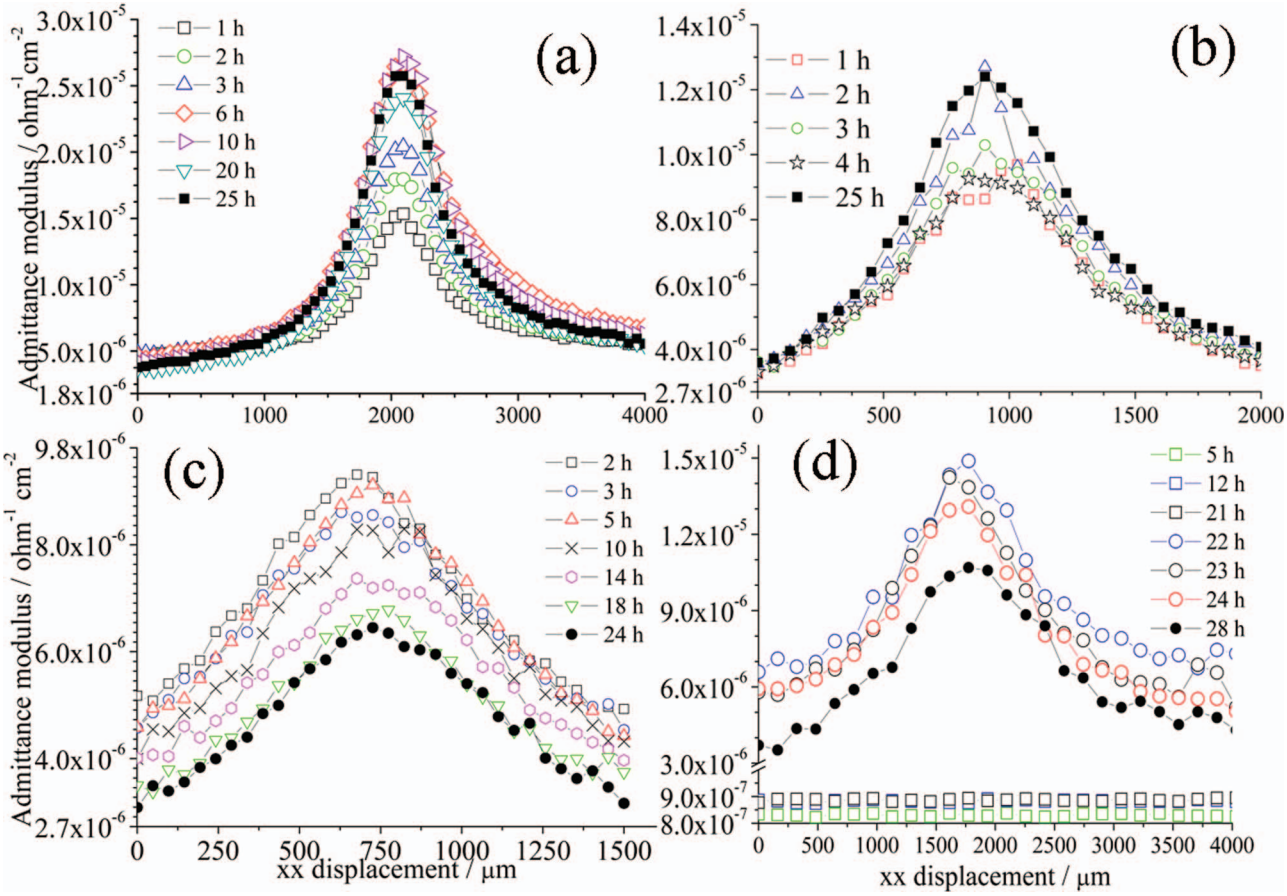

Figure 7. Admittance modulus versus xx displacement plots, at 77 Hz, of (a) only sol-gel and sol-gel modified with (b) MoNaX, (c) LaNaX and (d) mixture of LaNaX and MoNaX zeolite particles (La+Mo) after 24 hours of immersion in 1 mM NaCl solution.

It seems that during the initial 21 hours of immersion there was a different inhibiting mechanism, a cooperative effect between La and molybdate ions[29] that completely prevent the corrosion activity. After this initial time the corrosion process was slowed down by formation of La^{3+} containing compounds.[11] Thus, two inhibiting mechanisms could be operating, one for the first period of immersion, and a second one for longer immersion time. The complex interaction between La- and Mo-containing species determines this behavior.

SEM/EDS characterization of substrate/coating interface after corrosion.—Figure 8 shows SEM micrographs and EDS analyzes of a cross section of La+Mo coating after 2 weeks of immersion in 0.5 M NaCl solution. Five different areas were identified. EDS analysis on the area marked with 1 identified structural elements (C, O, Si and Zr) of the sol-gel matrix, Al element from the substrate, Na and Cl from the electrolyte solution.

EDS analysis on the white area identified with 3 at the coating/substrate interface shows a structure with Al, Cu, Mg, Mo, Na. In fact it is possible to observe in zones identified with 4 and 5 (Figure 8a and 8b) an interaction of molybdate with the Al substrate (Figure 8(a4) and (c4)) and with the intermetallic (Al(Mg,Cu)) (Figure 8(b5) and (c5)). Moreover on substrate surface, zone identified with 2, La, Mo and Na are identified on an Mg-containing area. In this area the amount of La was enough for the appearance of the three peaks of Kα energy. These experimental results indicate the release of molybdate and lanthanum from the enriched-zeolites and formation of a compound containing La, Mo and Na on the substrate surface (Figure 8(a2) and (c2)), which contributes to slow down (Figure 7d) the corrosion process. These observations showed that molybdate-containing species and La species were released and could interact with each other and the substrate, enhancing the coating protective action.

Release studies of La and Molybdate.— The La release as a function of pH of 0.5 M NaCl is shown in Figure 9a. The amount of La release from the zeolite microparticles is directly related to the pH of NaCl solution; the increase of pH causes the decrease of La

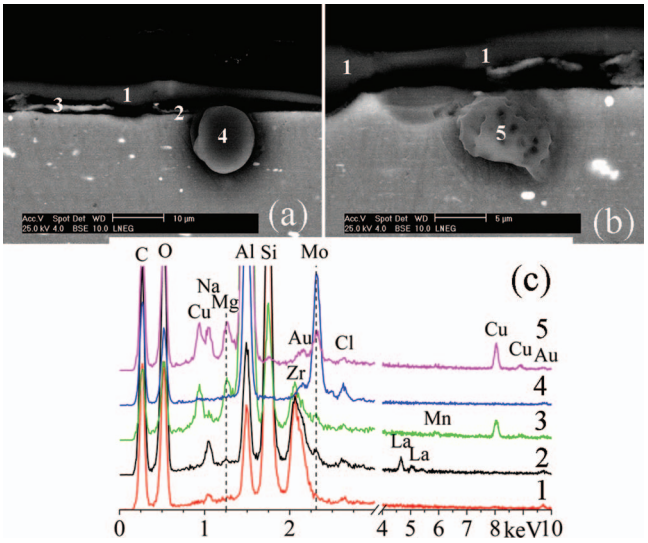

Figure 8. La+Mo coating after 2 weeks of immersion in 0.5 M NaCl solution; (a),(b) SEM micrographs and (c) EDS analysis on (1) sol-gel matrix; (2) substrate interface; (3) corrosion product; (4) substrate and (5) intermetallic particle (the dashed lines correspond to identification energy values of Na, Mo and Cu, respectively).

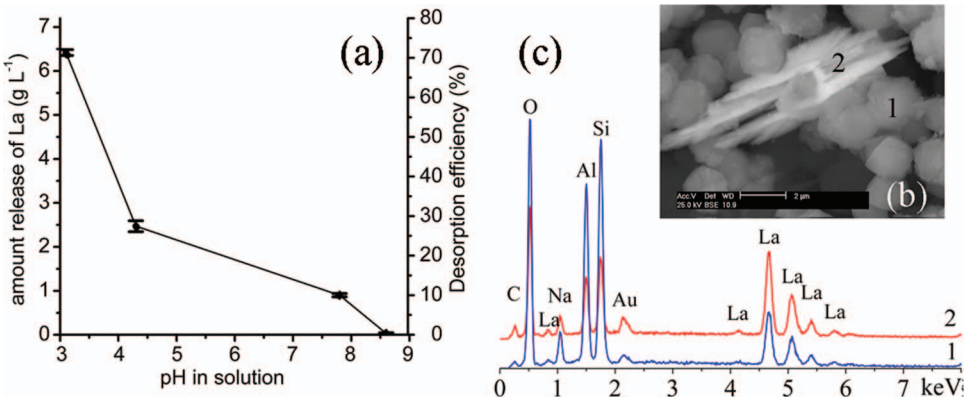

Figure 9. (a) Release of La from LaNaX zeolite microparticles as function of solution pH (error bars correspond to the standard deviations of experimental values), (b) SEM micrograph and (c) EDS analyzes of LaNaX zeolite powder after 48 hours of immersion in 0.5 M NaCl at pH = 8.6.

release. Figure 9 shows that for pH = 3 the amount of released La was 6.4 g L^{-1}, which corresponds to 71% of the La loaded in zeolite microparticles, and for pH = 8.6 was only 0.03 g L^{-1}, i.e. 0.33% of the loaded La was released. A SEM micrograph (Figure 9b) of LaNaX zeolite particles after 48 hours of immersion in 0.5 M NaCl at pH = 8.6 showed an assembly of feather-like structures uniformly attached to the zeolite microparticle. According to the EDS analysis (Figure 9c) this dendrite structure is a compound of lanthanum oxide (Figure 9(c2)). This fact can be explained in terms of the thermodynamic stability of La species formed at high pH.[30] According to the Pourbaix diagram, insoluble La oxides/hydroxides are formed at high pH.[30]

The enhancement of protection behavior had been previously observed in sol-gel coatings modified with Ce-enriched zeolites and modified with a mixture of Ce and Mo-enriched zeolites.[9,10] In these works it was possible to show that Ce release was triggered by the adsorption of Mg^{2+} and Cu^{2+} originated from the dissolution of intermetallic particles. So, due to the chemical similarity of Ce and La ions and to the type of the enriched zeolite microparticles used, it is expected that the La releasing process from LaNaX zeolites is identical to the process for Ce release. Otherwise, La^{3+} (5.6 and 2.8 wt%, Table I) present in sol-gel matrix would cause an early destruction of barrier properties of the film.[13]

On the other hand, the molybdate release from the zeolite microparticles is independent of solution pH and NaCl concentration, as shown in Table IV. The identical Mo concentration in all tests could correspond to the equilibrium (stoichiometric) values in the crystalline phases Na_2MoO_4 and $(NH_4)_2Mo_3O_{10}$ identified in the diffraction pattern of the MoOxNaX powder (Figure 2). The cations corresponding to $(NH_4)_2Mo_3O_{10}$ could also be released as the Ce[10] and La cations, i.e., at the expenses of Mg^{2+} and Cu^{2+} adsorption.

This fact can be explained by the complex aqueous chemistry of Mo, particularly Mo(VI). The structure and reactivity of Mo(VI) oxo-complexes are determined by the number and type of coordinated oxygen atoms or their protonated forms.[31] With the decrease in pH, the coordination number increases from 4 to 6, and octahedral Mo(VI) complexes start to prevail in the solution.[31,32] When the pH is less than 3, the cationic forms are predominant and they polymerize as the pH decreases (Mo^{3+}, MoO_2^{+}, $Mo_2O_5^{2+}$, $Mo_3O_8^{2+}$, etc).[30,33] However, at high pH the anionic forms of molybdenum are predominant and they tend to polymerize as the pH decreases (MoO_4^{2-}, $HMoO_4^{-}$, $Mo_7O_{24}^{6-}$, etc).[30,33] Since the loading process of the microparticles in zeolites occurred in acidified medium, the formation of $(NH_x)_y$-Mo_3O_{10} cations is possible and consequently their enclosure and release on zeolite structure as in the case of Ce+Mo coating.[10]

Table IV. Release of molybdate (concentration of Mo) from MoNaX zeolite microparticles after 48 hours of immersion as function of pH and concentration of NaCl solution.

	pH values 0.5 M NaCl			[NaCl] / M pH = 5.66		
[Mo] in solution / mol^{-1}	2.93	5.66	7.24	0.05	0.5	1.0
	5.48	4.39	5.26	5.70	5.12	4.49

Conclusions

Four different coating formulations were prepared: sol-gel films modified with commercial zeolite (NaX), enriched-zeolite (LaNaX or MoNaX) microparticles and sol-gel film modified with a mixture of LaNaX and MoNaX. All coatings had a zeolite concentration of 26.9 wt% (dry coating).

The sol-gel modified with the mixture of LaNaX and MoNaX zeolite microparticles (La+Mo) showed the highest pore resistance, resistance of intermediate oxide layer and charge transfer resistance of all coating formulations demonstrating an improvement on corrosion protection. LEIS measurements confirmed the synergistic action and showed total inhibition of corrosion during the initial 21 hours of immersion in 1×10^{-3} M NaCl.

The enhancement of protection was related to an effective protection effect due to a synergistic effect between molybdate and La^{3+} species that induces the formation of molybdenum oxide/hydroxide on IM particles. For latter immersion time, with the increase of pH, a La-Mo-Na compound was also formed slowing down the corrosion process.

The release studies indicated that the molybdate release mechanism is independent of the solution pH and of the NaCl solution concentration. The release of inhibitors, La and $(NH_x)_y$-Mo_3O_{10} cations, could be triggered by adsorption of Mg^{2+} and Cu^{2+} species resulting from dissolution of IM particles.

Acknowledgments

S.A.S. Dias acknowledges the FCT PhD grant SFRH/BD/46586/2008. The authors thank Mrs Teresa Magalhães for the XRD measurements and to Dr. Carlos Nogueira for the EDXRF and AAS measurements (LNEG).

References

1. N. N. Voevodin, N. T. Grebasch, W. S. Soto, L. S. Kasten, J. T. grant, F. E. Arnold, and M. S. Donley, *Prog. Org. Coat.*, **41**, 287 (2001).
2. N. N. Voevodin, V. N. Balbyshev, and M. S. Donley, *Prog. Org. Coat.*, **52**, 28 (2005).
3. M. L. Zheludkevich, I. M. Salvado, and M. G. S. Ferreira, *J. Mater. Chem.*, **15**, 5099 (2005).
4. M. L. Zheludkevich, R. Serra, M. F. Montemor, K. A. Yasakau, I. M Miranda Salvado, and M. G. S. Ferreira, *Electrochim. Acta*, **51**, 208 (2005).

5. D. G. Shchukin, M. Zheludkevich, K. Yasakau, S. Lamaka, M. G. S. Ferreira, and H. Möhwald, *Adv. Mater.*, **18**, 1672 (2006).
6. S. V. Lamaka, D. G. Shchukin, D. V. Andreeva, M. L. Zheludkevich, H. Möhwald, and M. G. S. Ferreira, *Adv. Funct. Mater.*, **18**, 3137 (2008).
7. S. A. S. Dias, S. V. Lamaka, C. A. Nogueira, T. C. Diamantino, and M. G. S. Ferreira, *Corros. Sci.*, **62**, 153 (2012).
8. M. L. Zheludkevich, J. Tedim, and M. G. S. Ferreira, *Electroch. Acta*, **82**, 314 (2012).
9. S. A. S. Dias, A. Marques, S. Lamaka, A. Simões, T. C. Diamantino, and M. G. S. Ferreira, *Electroch. Acta*, **112**, 549 (2013).
10. S. A. S. Dias, T. C. Diamantino, A. C. Bastos, D. De la Fuente, S. V. Lamaka, C. A. Nogueira, and M. G. S. Ferreira submitted in *Electroch. Acta.*
11. M. Bethencourt, F. J. Botana, J. J. Calvino, M. Marcos, and M. A. Rodríguez-Chacón, *Corros. Sci.*, **40**, 1803 (1998).
12. K. A. Yasakau, M. L. Zheludkevich, S. V. Lamaka, and M. G. S. Ferreira, *J. Phys. Chem. B*, **110**, 5515 (2006).
13. N. N. Voevodin, N. T. Grebasch, W. S. Soto, F. E. Arnold, and M. S. Donley, *Surf. Coat. Technol.*, **140**, 24 (2001).
14. M. Garcia-Heras, A. Jimenez-Morales, B. Casal, J. C. Galvan, S. Radzki, and M. A. Villegas, *J. Alloys Comp.*, **380**, 219 (2004).
15. G. Williams, H. N. McMurray, and M. J. Loveridge, *Electrochim. Acta*, **55**, 1740 (2010).
16. D. Álvarez, A. Collazo, M. Hernández, X. R. Nóvoa, and C. Pérez, *Mater. Sci. Forum*, **636–637** (2010).
17. H. N. McMurray and G. Williams, *Corrosion*, **60**, 219 (2004).
18. K. Arakami and N. Hackerman, *J. Electrochem. Soc.*, **116**, 568 (1969).
19. S. Kallip, A. C. Bastos, K. A. Yasakau, M. L. Zheludkevich, and M. G. S. Ferreira, *Electrochem. Comm.*, **20**, 101 (2012).
20. M. M. J. Treacy and J. B. Higgins, *Collection of simulated XRD powder pattern for zeolites*, p. 150-151, 4th Ed, Elsevier, New York (2001).
21. ICDD PDF# 36-0031 - Powder diffraction files (PDF) of International Centre for Diffraction Data (ICDD), 2013.
22. ICDD PDF # 26-0967 - Powder diffraction files (PDF) of International Centre for Diffraction Data (ICDD), 2013.
23. A. W. Burton, Power *Diffraction in Zeolite Science*, 1st edition, A. W. Chester and E. G. Derouane Editors, pp. 1–64, Springer, New York (2009).
24. B. Davó and J. J. de Damborenea, *Electrochem. Acta*, **49**, 4957 (2004).
25. M. A. Jakab, F. Presuel-Moreno, and J. R. Scully, *J. Electrochem. Soc.*, **153**, 244 (2006).
26. F. J. Presuel-Moreno, M. A. Jakab, and J. R. Scully, *J Electrochem. Soc.*, **152**, 376 (2005).
27. B. A. Shaw, G. D. Davis, T. L. Fritz, and K. A. Oliver, *J. Electrochem. Soc.*, **137**, 359 (1990).
28. W. D. Robertson, *J. Electrochem. Soc.*, **98**, 94 (1951).
29. S. R. Taylor and B. D. Chambers, *Corrosion*, **64**, 255 (2008).
30. M. Pourbaix, *Atlas of Electrochemical Equilibria in Aqueous Solutions*, 2nd edition, National Association of Corrosion Engineers, Houston (1974).
31. P. Tkac and A. Paulenova, *Separation Science and Technology*, **43**, 2641 (2008).
32. E. I. Stiefel, *Prog. Inorg. Chem.*, **22**, 1 (1977).
33. J. Aubry, D. Burnel, C. Gleitzer, and C. Molybdene, in P. Pascal (Ed), Complements au Nouveau Traité de Chimie Minéral, Masson Ed, 1979, vol 5.